Parametric and Metallurgical Investigation of Modified 3D AM 80 HD Steel for Wire and Arc Additive Manufacturing

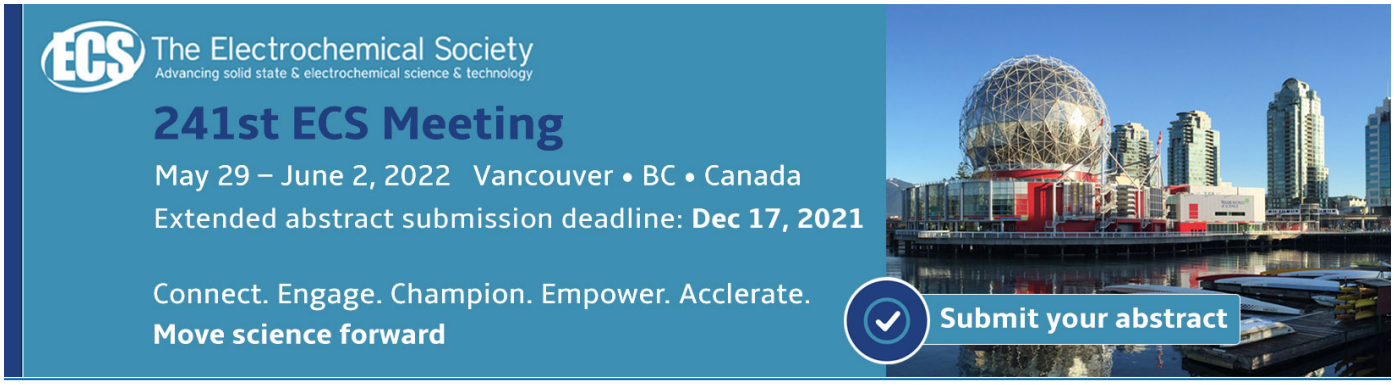

Parametric and Metallurgical Investigation of Modified 3D AM 80 HD Steel for Wire and Arc Additive Manufacturing

Zidong Lin[1,2], Kaijie Song[1,2], Wei Ya[3] and Xinghua Yu[1,2,*]

[1] School of Materials Science & Engineering, Beijing Institute of Technology, Beijing 100081, China.
[2] Beijing Institute of Technology Chongqing Innovation Center, Chongqing 401120, China.
[3] Rotterdam Additive Manufacture Fieldlab (RAMLAB), Scheepsbouwweg 8 F6, 3089JW Rotterdam, The Netherlands.
Email: xyu@bit.edu.cn

Abstract. Wire and arc additive manufacturing (WAAM) is an advanced 3D printing method for metallic materials on the foundation of traditional arc welding processes. WAAM is regarded as a proper way to manufacture large-dimensional metallic parts with the combination of high deposition rate and low cost. In this research, a specifically designed and manufactured low carbon high strength steel (Grade 3D AM 80 HD) wire, equivalent to a composition of AWS ER 110S-1 wire, was deposited using WAAM to print a muti-beads wall aiming to explore its feasibility for heavily loaded marine applications. A parametric investigation was proceeded to find the optimal deposition voltage and overlap ratio. A vertical position compensation method was adopted to optimize the step-up distance for welding torch between neighboring layers. Microstructure of the deposited component was characterized and also indicated by Thermal-Calc Software, followed by the measurement of hardness and prediction of tensile strength. Furthermore, a comparison of tensile strength of the WAAMed 3D AM 80 HD wall, 3D AM 80 HD wire, AWS ER 110S-1 wire, and a WAAMed wall produced by wire manufacturer (Voestalpine Böhler Welding Corporation) was conducted.
Keywords. Wire and arc additive manufacturing (WAAM), Steel, Parametric investigation, Microstructure, Mechanical properties.

1. Introduction

Wire and arc additive manufacturing (WAAM) is an advanced and cost-effective technique that can directly produce near-net-shape components with complex shapes and large-scale dimensions. It normally employs a welding arc as heat source and metallic feeding wire to be consumable. Due to its advantages of high deposition rate, short lead time, and high material utilization, WAAM has been broadly applied in various fields [1-3]. Although WAAM is an invented derivative based on traditional welding methods such as gas metal arc welding (GMAW), gas tungsten arc welding (GTAW), and plasma arc welding (PAW), the details related to traditional welding are not necessarily suitable for WAAM. To the best knowledge of the authors, the existing welding consumables have not been assessed completely for good applicability of WAAM. For instance, some elements such as silicon are excessively added in steel welding wires for improving the melt pool flow and protection. More silicon in the wire could increase both tensile strength and wire resistivity so that the melting efficiency could be improved [4]. However, numerous addition of silicon can lead to the formation of

relatively thick oxide layers on surface of beads, which causes arc initiation failure and defects. It requires interventions from the operator to clean it manually, which is not desirable for the automated robotic WAAM process. Besides, the market demand for special alloys is still not commercially attractive [5] due to the small volumes required for WAAM at the moment. This further leads to a limited number of institutes and researchers who pay attention to developing alloys dedicated to WAAM process. As a result, it will be interesting and helpful to tailor the weld consumable chemical composition for WAAM products. In this study, a low carbon high strength steel wire was designed and studied for the candidate consumable used in GMAW-based WAAM process. The chemical composition of the designed wire was modified based on the same grade of commercial welding wires to satisfy the special interest for manufacturing heavily loaded maritime or construction structures. A parametric investigation was proceeded to investigate optimal deposition parameters. Microstructure at different locations of the WAAM deposited wall was characterized with the assistance of Thermal-Calc Software. Tensile strength of the WAAMed wall was predicted based on measured hardness, followed by proof of a WAAMed wall produced by the wire manufacturer (Voestalpine Böhler Welding Corporation). Besides, tensile strength of the as-deposited 3D AM 80 HD wall was also compared to 3D AM 80 HD wire and AWS ER 110S-1 wire.

2. Materials and Methods

The material of used base plate was S355 (EN 10025-2:2004) steel [6] and the dimension was $250 \times 60 \times 10$ mm^3. New designed 3D AM 80 HD (Voestalpine Böhler Welding Corporation) wire with a diameter of 1.2 mm was adopted as filling feedstock. It is a high-performance, iron-based solid wire, aimed to provide process stability, reduced silicate formation, and high-temperature resistance. It was modified from the same grade traditional welding wire equivalent to AWS ER 110S-1 and the corresponding alloying elemental contents are listed in table 1. For the 3D AM 80 HD, the chemical composition referring to the composition of the deposited metal was measured by optical emission spectroscopy (OES). Prior to deposition, the base surface was cleaned with an acetone ($(CH_3)_2CO$) solution.

Table 1. The composition of materials used in this research (*wt.%*).

Materials	C	Si	Mn	Cr	Mo	P	S	Cu	Ni
3D AM 80 HD	0.09	0.40	1.70	0.35	0.60	0.01	0.01	0.25	2.00
ER 110S-1	0.09	0.2-0.55	1.4-1.8	0.5	0.25-0.55	0.01	0.01	0.2	1.9-2.6
S355	0.2	0.55	1.6	/	/	0.025	0.025	0.55	/

The deposition experiment was implemented with a robotic arm produced by Panasonic Company (figure 1(a)) and a welding power source integrated by Valk Welding. The professional software employed to design and form deposition tool paths was invented by Autodesk PowerMill (Autodesk B.V, Hoofddorp, The Netherlands). As can be seen, the experimental arrangement to realize high-quality deposition is illustrated in figure 1(b). The welding torch was placed vertically to the base plate (PA position). The printing strategy, i.e., reversing the deposition direction for each layer as shown in figure 1(c), was applied to avoid the height difference resulted from arc start and arc stop zones. In this study, a small wall ($100 \times 20 \times 10$ mm^3) was deposited to characterize and investigate the WAAM material quality. The deposited wall contains five layers and each layer consists of five partially overlapped beads. To acquire the optimized welding conditions of the wall, the optimization of WAAM experiments needs to be carried out. A parametric test was proceeded through ramping up the voltage (18-22 V) in order to pick up proper deposition conditions based on good bead appearance, an appropriate aspect ratio (width to height ratio), and the corresponded step-up distance (the distance that the torch is lifted after printing per layer alone vertical height direction). After printing every layer, the wall experienced an air cooling process until the top surface was measured to be at ambient temperature, and the contact tip-to-work distance (CTWD) was then hoisted 1 mm higher. The

schematic of ramping deposition test is shown in figure 2. The related deposition parameters are listed in table 2.

The samples of the as-deposited wall were prepared for metallurgical and mechanical investigations. The cross section of wall was etched by Nital etchant consisted of 98% ethanol and 2% HNO_3 for optical microscopy (Keyence VHX-5000, Osaka, Japan). Vickers hardness (HV_5, with 0.5 kgf) was measured on a cross section of the wall, in the direction from the highest point towards the base, using a Struers DuraScan-70 machine (Struers Inc., Cleveland, OH, USA).

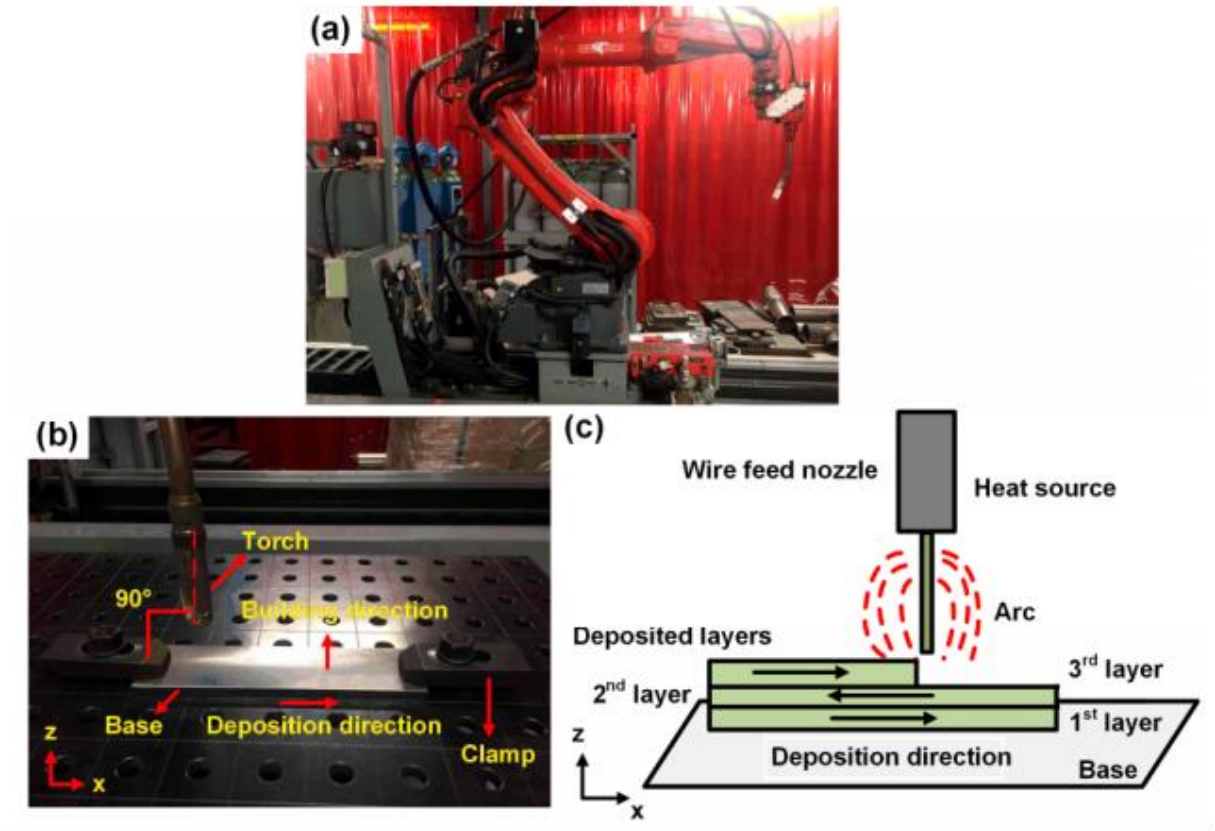

Figure 1. Experimental robot, set-up, and deposition schematic: (a) panasonic robotic arm, (b) deposition arrangement, (c) deposition strategy.

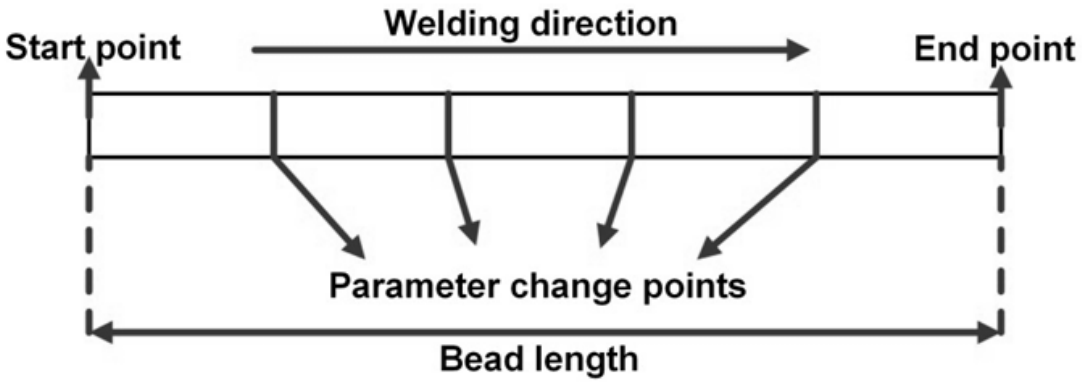

Figure 2. Schematic of ramping deposition test.

Table 2. Related deposition parameters.

Contact tip-to-work distance (CTWD)	1 [mm]
Polarity	Direct current, reversed polarity (Wire: positive, base: negative)
Stick out length	13 [mm]
Pulse mode	No pulse
Molten droplet transfer mode	Spray
Gas flow rate (20% CO_2, 80% Ar)	18 [L min^{-1}]
Inter-pass temperature	298 [K]
Wire feed speed (WFS)	6.5 [m min^{-1}]
Voltage (U)	18-22 [V]
Deposition speed (v)	1 [m min^{-1}]

3. Results and Discussion

3.1. Optimization of Single Bead, Overlap Ratio, and Step-up Distance

The result of ramping deposition test is shown in figure 3(a), from which the bead appearance under different voltage conditions can be seen. Overall, there is no significant difference for the entire deposited bead due to small voltage variation range. Glossy metallic color indicates good oxidation prevention during deposition process. However, some tiny features caused by voltage change still can be observed, which could affect subsequent deposition quality. With the voltage increasing from 18 V to 21 V, the continuity near the weld toe becomes deteriorated, which is indicated by the black rectangle marks. Such discontinuity also locates at the junction region of the neighboring overlapped beads, which increases the possibility of unfilled holes and cracking. As voltage further increased to 22 V, patterns on surface (black triangle in figure 3(a)) of the bead become deep and apparent. This was caused by severer violent melt pool contributed by the comprehensive influence of high heat input and fast deposition speed. Therefore, a voltage equal to 18 V was selected for subsequent muti-beads and multi-layers deposition. With this relatively lower heat input, the inter-layer dwell time can be greatly reduced to improve production efficiency. Besides, the cooling rate will be also increased, which benefits more formation of martensite to enhance mechanical strength. The average bead dimensions at the voltage range of 18 V were measured. The bead height was 1.87 mm and the bead width was 7.327 mm, which gave an aspect ratio of 3.58 at the lower border of the good weld shape [7].

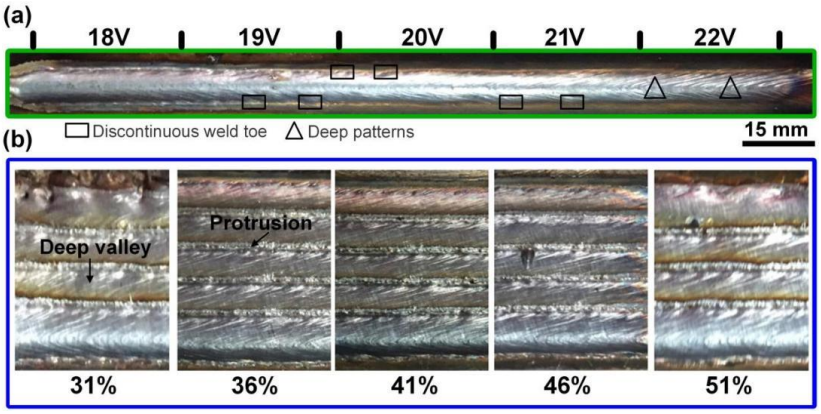

Figure 3. Optimization results of single bead and overlapped beads: (a) ramped single bead, (b) overlapped beads with different overlap ratios.

Figure 3(b) illustrates the profile of five overlapped beads with different overlap ratios ($1-\frac{\text{Distance between the center line of two neighboring beads}}{\text{Bead width}}$). From the samples with 31% and 51% overlap ratios, a deep valley exists between neighboring beads, resulting in relatively more material filling in this area during the deposition of the next layer. This ununiformed material distribution will cause an uneven layer surface and such phenomenon will become worse with the increased number of deposited layers. Small protrusions on surface couldn't be removed because of limitation of the material fluidity. The appearance of samples with overlap ratios of 36%, 41%, and 46% is similar. Considering that higher overlap ratios such as 41% and 46% would lead to longer time for printing each layer, 36% was chosen as the optimal overlap ratio.

Based on previously determined deposition parameters for single bead and optimal overlap ratio, the proper step-up distance between neighboring layers can be studied to avoid large deviation from the designed component. However, as the number of deposited layers increased, the wire tip can deviate from the surface of the previously deposited layer. This means that the Contact Tip-to-Work Distance (CTWD) became larger and larger. The possible explanations are (i) Partially melting of previous layers increases the melt pool width and decreases the melt pool height, (ii) The melt at the edge sides of the wall is flowing down due to gravity. Therefore, to be able to deposit with a constant distance between the wire tip and surface of the previous layer, an optimal step-up distance needs to be investigated. In this study, a vertical position compensation method for welding torch was adopted. A wall, with 5 layers with each 5 overlapped beads, was deposited. The main procedure flow is shown in table 3. By doing so, the influence of base material (dissimilar to deposited material) was taken into account and the step-up distance is optimized to be 1.91 mm.

Table 3. The main procedure flow of vertical position compensation method.

Procedures	Works
Step 1	Deposit the 1st layer and get the layer height h_1
Step 2	(i) Move the welding torch to the surface of the 1st layer (ii) Deposit the 2nd layer and calculate the height of the 2nd as h_2 (iii) The welding torch is continuously increased by h_2 to deposit the 3rd ~ 5th layers
Step 3	(i) The total height of 5 layers as H_5 (ii) The height of 2nd ~ 5th layers is H_5-h_1 (iii) The theoretical value of the total height of 2nd ~ 5th layers is $4h_2$ (iv) The difference ΔH is $h_1+4h_2-H_5$
Step 4	The step-up distance is optimized and equal to $h_2-(h_1+4h_2-H_5)/3$

3.2. Microstructural Characterization

The microstructure of the 3D AM 80 HD wall deposited by WAAM is shown in figure 4(a). The zoomed figures are respectively taken from the top region (5th layer), middle region (3rd layer), and bottom region (1st layer), which are marked with red rectangles in figure 4(a). In general speaking, there is a microstructural variation between different layers. The entire wall is composed of pearlite, martensite, and carbides. Due to fast heating and cooling rate plus rapid deposition rate, martensite will form, which is indicated by the microstructure of top region (5th layer) as shown in figure 4(d). However, when printing the final layer (5th layer), previous layers experience different tempering temperatures so that the lath shape and size of martensite are different. This can be clearly shown by the tempered martensite in figure 4(c), whose lath dimension is larger than that of top region. Besides, partially formed martensite undergoes reverse transformation so that the nucleation of cementite forms on dislocations, resulting in that martensite transforms to pearlite [8]. At the bottom region (1st layer) of the wall, the microstructure experienced the longest tempering time, thereby martensite completely transformed to pearlite. Long-term tempering also promotes the precipitation of carbides in tempered martensite or ferrite matrix and further experience the coarsening process. From the phase composition

shown in figure 5, several kinds of carbides can form while $M_{23}C_6$ which accounts for the highest content at ambient temperature, is the most possible. KSI carbides and M_7C_3 carbides are also promised to retain from their high formation temperature to ambient temperature. This is due to fast cooling rate and a bit thermal cycles to lower the probability of carbides dissolving and transformation. The grain size at bottom region is smaller than that at top region owing to repeated thermal cycles and more rapid cooling at the bottom of the wall. The slower dissipation of heat as the distance from the baseplate increases and heat builds up in the wall allows for grain coarsening at the top of the wall [9].

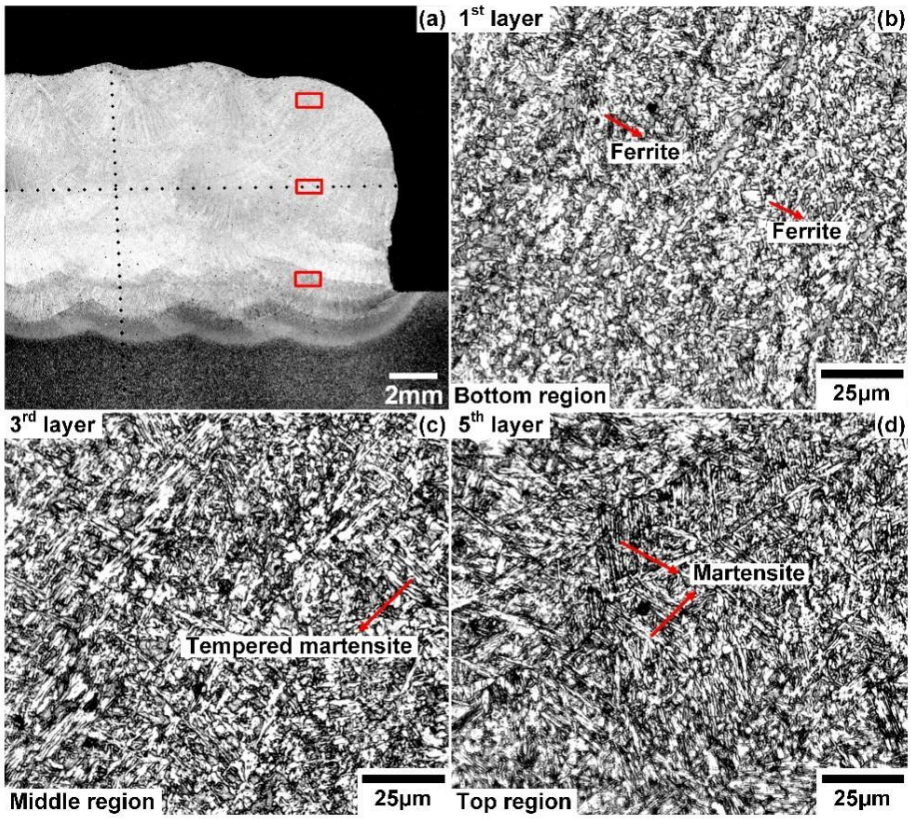

Figure 4. Microstructure of the 3D AM 80 HD wall deposited by WAAM: (a) cross section, (b) 1st layer, (c) 3rd layer, (d) 5th layer.

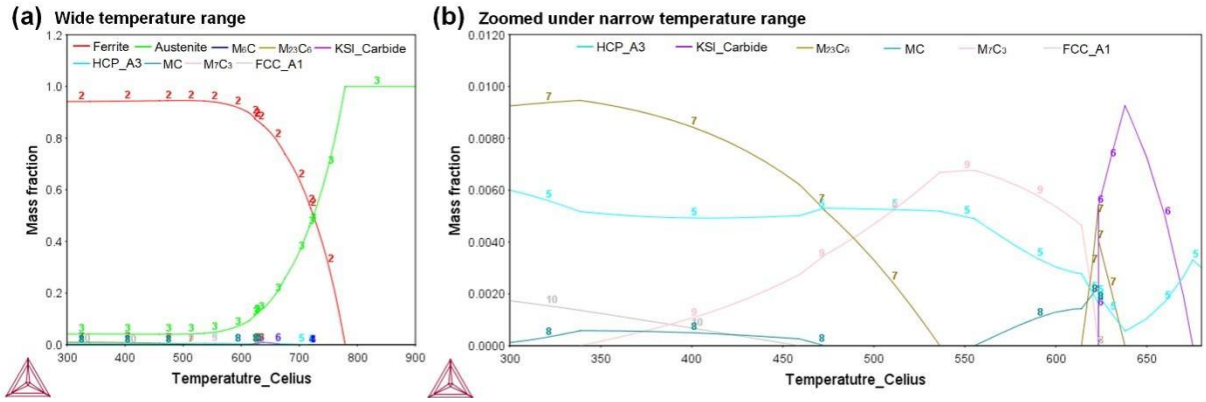

Figure 5. Phase composition for 3D AM 80 HD wire computed by Thermal-Calc: (a) wide temperature range, (b) zoomed under narrow temperature range.

3.3. Hardness and Tensile Strength

The indentation path for measuring hardness is shown in figure 4(a) and the measured hardness of the 3D AM 80 HD wall is shown in figure 6. The hardness in the horizontal direction is measured in the middle height (3rd layer) of the wall. The hardness fluctuation is large up to 75 HV, which may indicate the strength properties are not uniform in horizontal direction. The hardness near the edge is higher than that in middle, which is contributed by a faster cooling rate promoted by air convection. The hardness of the start point is found to be lower than the end point. This great difference might due to the fact that the test start point is too far from the left edge of the sample. In addition, the hardness in vertical direction decreases from top to bottom regions, resulted by the microstructures at corresponding locations. At bottom regions, finer grains and precipitated carbides respectively conduce hardness by means of the Hall-Petch relationship and hindering dislocation movement for strain hardening.

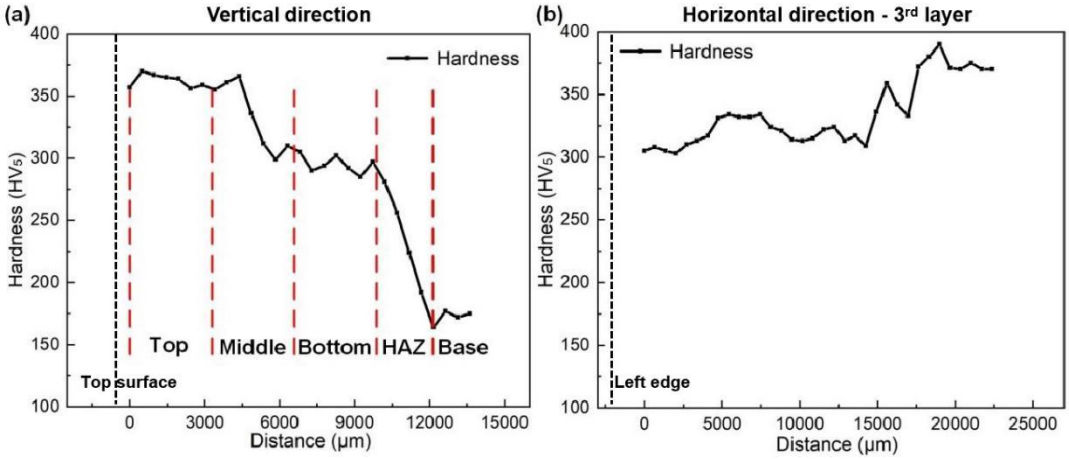

Figure 6. Hardness of the 3D AM 80 HD wall deposited by WAAM: (a) vertical direction, (b) horizontal direction - 3rd layer.

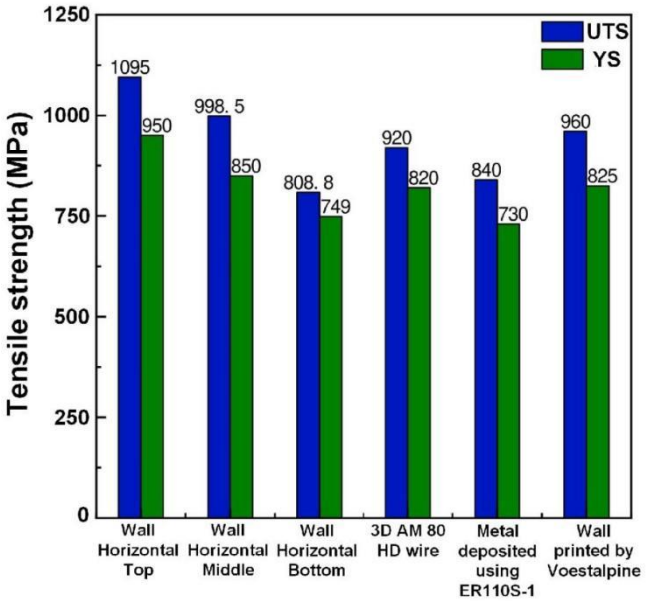

Figure 7. Tensile strength of deposited 3D AM 80 HD wall, 3D AM 80 HD wire, and AWS ER 110S-1 wire.

According to E.J. Pavlina et al. [10] and G. Rosenberg [11], both tensile strength and yield strength for steel shows a clear linear relationship with the diamond pyramid hardness, which respectively follows equation (1) and equation (2). Due to anisotropy of the mechanical strength for the WAAMed components, it should be noted that the predicted tensile strength is in horizontal direction. Based on the obtained hardness results, the average hardness in horizontal direction including top, middle, and bottom regions is 362 HV, 327 HV, and 292 HV while the average hardness in vertical direction is 334 HV. As a result, the ultimate tensile strength (UTS) and yield strength (YS) in horizontal direction can be predicted and calculated out as shown in figure 7. As a comparison, the tensile strength of 3D AM 80 HD wire, the same grade wire AWS ER 110S-1, and a 3D AM 80 HD wall printed by the wire manufacture (Voestalpine Böhler Welding Corporation) are also listed in figure 7. Firstly, it can be concluded that the 3D AM 80 HD wire has a strength superiority compared to the same grade wire AWS ER 110S-1. The tensile strength decreases from the top to bottom region, which has the same trend with other WAAMed steel components [11]. In top and middle region of the 3D AM 80 HD wall deposited by WAAM, both UTS and YS are higher than that of 3D AM 80 HD wire. This can also be proved by the wall WAAM-printed by Voestalpine as indicated in figure 7. The cause of lower strength at the bottom region of the wall is reverse transformation of martensite mentioned before.

$$UTS = 92.754 + 2.77\ HV \quad (1)$$

$$YS = -90.7 + 2.876\ HV \quad (2)$$

4. Conclusions

In this study, the microstructure and mechanical properties of WAAM components deposited using 3D AM 80 HD solid wires were investigated. The 3D AM 80 HD wall performed superior structural integrity and mechanical properties, which is attractive for many industrial applications. From the results and discussion mentioned previously, the following conclusions can be drawn:

- The deposition voltage, overlap ratio, and step-up distance to print 3D AM 80 HD wall were optimized by parametric investigation.
- A vertical position compensation method was introduced to determine the step-up distance between neighboring layers.
- The mechanical properties comparison between WAAM produced 3D AM 80 HD component, 3D AM 80 HD wire, and the part deposited using ER 110S-1 was proceeded. Both hardness and tensile strength (except for the strength at bottom region of the wall) of the WAAMed wall are higher or comparable with the ones coming from 3D AM 80 HD wire and WAAMed parts deposited using ER 110S-1 wire.
- The hardness fluctuation from bottom to top region of the wall is within 281 HV to 370 HV.
- Pearlite, martensite, and carbides are present in the constructed wall. The computed results by Thermal-Calc indicated that the species of precipitated carbides are possible to be $M_{23}C_6$, M_7C_3, and KSI carbides. Martensite experienced reverse transformation to pearlite under tempering process. In addition, the repeated thermal cycles and more rapid cooling rate at bottom regions caused fining of grains.

Acknowledgments

The work is sponsored by Beijing Institute of Technology Young Scholar Startup Program. Authors would like to acknowledge support from Experimental Center of Advanced Materials (ECAM) of Beijing Institute of Technology and National Key Laboratory of Science and Technology on Materials under Shock and Impact.

References

[1] Lin Z, Ya W, Subramanian V, Goulas C, Benedetto C, Hermans M and Pathiraj B 2020 *The International Journal of Advanced Manufacturing Technology* **111** 411-426.
[2] Lin Z 2019 http://resolver.tudelft.nl/uuid:ed3515f3-b43a-4cdc-9f11-2e249c97bbed.

[3] Lin Z, Goulas C, Ya W and Hermans M 2019 *Metals* **9** 673.
[4] Xu X, Feng Y, Liu D, Wang Y, Li W, Yan K and Li B 2016 *In MATEC Web of Conferences* **67** 05002.
[5] Frazier E 2014 *Journal of Materials Engineering and Performance* **23** 1917-1928.
[6] Corus 2004 https://www.tf.unikiel.de/matwis/amat/iss/kap_9/articles/en_steel_standards.pdf.
[7] Ya W, Hernández-Sánchez F, Pathiraj B and Veld A 2013 *In International Congress on Applications of Lasers & Electro-Optics* **2013** 453-462.
[8] Zhao Y, Xiang Z, Tan Y, Ji X, Zhang L, Zhang F and Xiang S 2019 *Materials* **12** 396.
[9] Wang Z, Palmer T and Beese A 2016 *Acta Materialia* **110** 226-235.
[10] Pavlina E and Van Tyne C 2008 *Journal of Materials Engineering and Performance* **17** 888-893.
[11] Gaško M and Rosenberg G 2011 *Mater. Eng*, **18** 155-159.